Probing ice VII crystallization from amorphous NaCl–D 2 O solutions at gigapascal pressures

A.-A. Ludl, L. E. Bove, D. Corradini, M. Saitta, M. Salanne, C. L. Bull, S. Klotz

PCCP

PAPER

Probing ice VII crystallization from amorphous NaCl–D_2O solutions at gigapascal pressures†

Cite this: *Phys. Chem. Chem. Phys.*, 2017, **19**, 1875

A.-A. Ludl,*[ab] L. E. Bove,*[ae] D. Corradini,[c] A. M. Saitta,[a] M. Salanne,[c] C. L. Bull[d] and S. Klotz[a]

Received 27th October 2016,
Accepted 6th December 2016

DOI: 10.1039/c6cp07340a

We probe the possible inclusion of salt (NaCl) in the ice VII lattice over the pressure range from 2 to 4 gigapascal. We combine data from neutron diffraction experiments under pressure and from computational structure searches based on density functional theory. We observe that the high density amorphous precursor (NaCl·10.2D_2O) crystallises during annealing at high pressure in the vicinity of the phase boundary between pure ices VII and VIII. The structure formed is very similar to that of pure ice VII. Our simulations indicate that substituting water molecules in the ice VII lattice with Na^+ and Cl^- ions would lead to a significant expansion of the lattice parameter. Since this expansion was not observed in our experiments, the ice crystallised is likely to be pure D_2O or contains only a small fraction of the ions from the salt solution.

1 Introduction

In a previous study we have shown that NaCl solutions close to the eutectic composition (NaCl·10.2D_2O) can vitrify at ambient pressure provided that sufficiently fast quenching rates (cooling rate $>10^3$ K s^{-1}) are employed.[1] Upon compression up to 4 gigapascal and subsequent temperature annealing under pressure, the amorphous NaCl·10.2D_2O system undergoes a smooth densification associated with the gradual increase of the number of neighbour molecules/ions in the hydration shell of the Na^+ ion.[1]

This behaviour contrasts with the one observed in LiX solutions close to the eutectic composition (LiCl·6D_2O and LiBr·5.5D_2O) where an abrupt increase in the Li^+ ion coordination was observed when following the same thermodynamic path.[3] Combining the results of molecular dynamics simulations based on classical polarisable potentials[4,5] and neutron diffraction experiments,[6] we have shown that the behaviour of such solutions upon compression is essentially driven by the structure of the hydration shells of the respective cation.[1] The first neighbours' shell of Li^+ has a tetrahedral structure at ambient pressure, which breaks up near 2 gigapascal to form an octahedral shell, giving rise to the observed sudden change in density.[3] In the case of Na^+, the shell is already octahedral at ambient pressure. The compression leads to a progressive distortion of the octahedra around Na^+ and to the formation of irregular polyhedra of 7 and 8 closest neighbours as

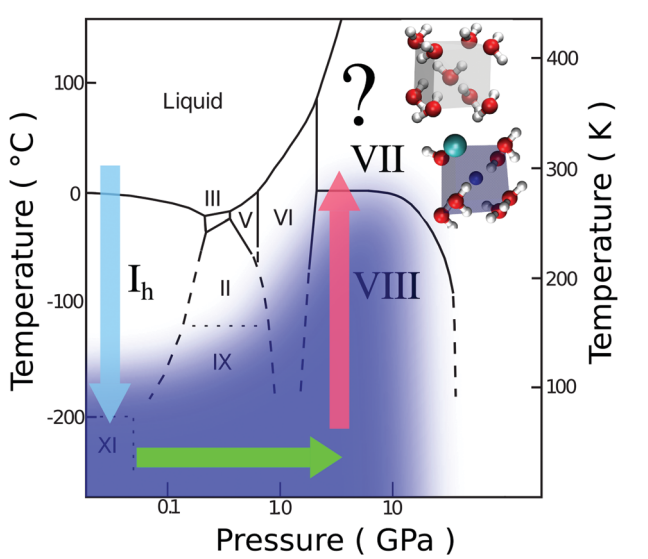

Fig. 1 The thermodynamic path along which NaCl·10.2D_2O has been studied by neutron diffraction and computer simulations. The blue coloured region indicates the domain in which the amorphous phase of NaCl·10.2D_2O has been observed. The phase boundaries of crystalline ices are based on those of ref. 2. Arrows: blue: quench at ambient pressure, green: compression at 80 K, red: annealing under pressure (2 to 4 GPa). Insets: Lattice of pure ice VII (above) and ice VII with substitutional ions (below).

[a] *Sorbonne Universités, UPMC Univ. Paris 06, CNRS UMR 7590, IRD, MNHN, IMPMC, Paris, France. E-mail: alexander.ludl@gmail.com, livia.bove@impmc.upmc.fr*
[b] *Departament d'FMC, Universitat de Barcelona, Av. Diagonal 645, E-08028 Barcelona, Spain*
[c] *Sorbonne Universités, UPMC Univ. Paris 06, CNRS UMR 8234, PHENIX, Paris, France*
[d] *ISIS Facility, STFC Rutherford Appleton Laboratory, Harwell Science & Innovation Campus, Harwell Oxford, Oxon, OX11 0QX, UK*
[e] *EPSL, Institute of Condensed Matter Physics, EPFL, CH-1015 Lausanne, Switzerland*

† Electronic supplementary information (ESI) available. See DOI: 10.1039/c6cp07340a

pressure increases. This process explains the gradual densification observed in the NaCl·10.2D_2O system.[1]

We have shown that in the case of LiCl and LiBr solutions[6,7] such high-density amorphous structures act as precursors for a crystalline ice phase which is formed upon further annealing of the temperature under pressure. The structure of this salty ice closely resembles the one of pure ice VII but large amounts of Li^+, Br^- and Cl^- ions are included in the lattice, either interstitially (Li^+) in octahedral voids or by substituting water molecules on sites of the ice VII lattice. The presence of ions prevents water molecules from orienting and the resulting crystal is orientationally disordered.[6] The presence or absence of ions has also been shown to control the occurrence of phase transitions and is linked to quantum effects in phases of water.[8,9] The structure of magnesium chloride hydrates, in particular the high-pressure hydrate MgCl·2.10D_2O at 2.5 gigapascal, also includes Mg^{2+} in octahedral geometry[10] similar to what is observed for Li^+.

The difference in the behaviour of NaCl-solutions under compression raises the question of whether Na^+ ions can also be included in ice VII or not. In particular, taking into account the local structure of the amorphous precursor, one would expect that Na^+ ions could substitute water molecules and occupy the oxygen sites in the body centered cubic lattice (bcc). A recent experiment performed at much higher pressures using Raman spectroscopy, up into the megabar range, on ice phases nucleated from dilute NaCl solutions (NaCl·52D_2O) suggested that at least part of the NaCl was included in the ice lattice, as the hydrogen bond symmetrisation behaviour was different from the one expected for pure ice.[9,11] However, this hypothesis needs to be corroborated by a direct determination of the crystal structure of the solution produced under high pressure.

In this study, we explore the possible inclusion of NaCl under annealing at pressures between 2 and 4 GPa, *i.e.* in the stability domains of ice VIII and ice VII as shown in Fig. 1. This range of pressures is highly relevant for the modelling of icy bodies in our solar system[12,13] and is easily accessible to neutron diffraction experiments which allow a direct determination of the system's structure even in the presence of inclusions of light elements.

The paper is organised as follows. In Section 2 the experimental high-pressure diffraction methods and the computational methods used in this study are described. In Section 3 the results on the inclusion of NaCl in ice VII are presented.

2 Methods

2.1 High-pressure neutron diffraction experiments

Solutions of NaCl in D_2O were prepared by mixing de-hydrated NaCl salt with pure (99.75%) D_2O. Composition close to the eutectic, *i.e.* R = 10.2 in D_2O, was chosen in order to maximize the amorphization ability of the solution.[1,14] The amorphous phase was produced by fast quenching of the solution to liquid nitrogen temperature (77 K) with an estimated cooling rate of 10^4 K s^{-1}. This high quenching rate was obtained by spraying micro droplets, diameter ≈10 to 30 μm, of the solution on a cold plate maintained at 77 K under vacuum.[1,15] Subsequently the powder was compacted to lenticular shaped pellets under liquid nitrogen for the loading of the high-pressure cell.

We report data on three samples of NaCl·10.2D_2O which were studied by high-pressure diffraction experiments carried out at the time-of-flight PEARL beamline of the UK pulsed neutron facility ISIS in Didcot.[16] These samples will be called sample A, B and C in the following. They were annealed at pressures in the range of 2 to 4 GPa. The pellets of the samples were split into two hemispheres and a small piece of lead was placed in between them to serve as a pressure calibrant.[17] The reassembled pellets were subsequently loaded into pre-cooled null-scattering titanium–zirconium ($Ti_{0.677}Zr_{0.323}$) encapsulating gaskets[18] at ≈80 K, and placed between pre-cooled sintered diamond anvils, which where clamped before insertion into a pre-cooled V3 Paris-Edinburgh (PE) press. The initial sample volume was approximately 40 mm^3. A liquid nitrogen cryostat was used in this experiment to cool the whole PE press. The details of the cryogenic set-up are described in ref. 19. The vanadium standard for this experiment was a sphere of vanadium of the same size as the samples, which was loaded into the gasket and the PE press in the same set-up as the samples at ambient pressure and temperature.

The gaskets were sealed by applying a load of 80 kN on the anvils. The loading and subsequent sealing of the gaskets under liquid nitrogen leads to a small amount of liquid N_2 trapped in the sample chamber. Under high pressure, this nitrogen crystallizes and produces small Bragg reflections (see further below) which serve as pressure marker, for scans where lead peaks are absent, since the equation of state of the solid phases of nitrogen is well known. In sample C lead peaks and nitrogen peaks were visible, which allowed to confirm that the pressure markers agree to within 0.1 GPa. There is no evidence from our data, nor from the literature, that nitrogen interacts with ice VII. The first scans were recorded at the initial load at ≈90 K, corresponding to 0.5 GPa on the sample. Then pressure was increased in steps of about 0.5 GPa up to ≈3 GPa in sample A, ≈2 GPa in sample B and ≈4 GPa in sample C. Thereafter the samples were slowly heated to room temperature at a rate of ≈20 K h^{-1} with diffraction data continuously collected along the paths shown in Fig. 1. The load was reduced at 185 K in order to prevent pressure increase on the sample upon warming. Data were collected continuously, with time slices of 1 hour being summed for the points along the thermodynamic path followed during the experiment. The scans used to determine the lattice parameters of ice (Table 2) were chosen as those with stable temperature and pressure.

The recorded data contain the peaks of the sintered diamond anvils, which were fitted together with the other phases present. The Rietveld fits of the crystalline phases in these diffractograms were performed using GSAS and its graphical interface EXPGUI, using time-of-flight profile function 1.[20–22] The structures of ices VII and VIII were taken from ref. 23 and 24. The phase diagram of ref. 25 was used to determine the pressure in the sample chamber by fitting the β and δ phases of N_2, whose

structures were taken from ref. 26 and 27 respectively. Where lead peaks were visible, these were fitted and the EOS of ref. 17 was used. The estimated error in the pressure determination is 0.2 GPa. A figure showing tick-marks for peaks of all phases is shown in the ESI.†

Before compression the samples also contained a fraction ($\approx$10%) of hexagonal ice visible in the diffractograms as Bragg peaks. This phase transforms during compression and its peaks shift, until further compression induces amorphization of the crystalline part into a high density amorphous (HDA) phase, which recrystallizes at around 2 GPa into the ice VIII phase.[28]

2.2 Simulation methods

Density functional theory based simulation methods were used in order to complement our experimental study. We applied a screening method based on ref. 29 which is adapted from ref. 30 and 31. A 3 × 3 × 3 super-cell of ice VII containing 54 water molecules was used to obtain a set of 100 000 candidate structures for salty ice VII.

Given that the sizes of sodium and chlorine ions are of the same order of magnitude as that of water, we expect both of them to substitute water molecules on sites of the ice VII lattice. Two cases were studied, in the first case 8 ions were substituted into the box (R = 11.5) and in the second case 2 ions were substituted (R = 52).‡ We proceeded in four steps:

(1) We generated sets of structures by randomly substituting 8 ions for water molecules and evaluating their energies with the polarizable ion model (PIM)[5] and a water model by ref. 4 in CP2K.[32] This was done for a set with 8 ions of $\approx$100 000 configurations.

(2) Then we evaluated the DFT energies of the 1000 configurations of lowest energy using CP2K.

(3) We did geometry optimisation using DFT on 200 configurations chosen randomly among the set of step 2, keeping the cell vectors fixed.

(4) We performed cell optimisation using DFT on 13 cells at 4 GPa.

A box of pure ice VII and a box with 8 ions substituted are shown in Fig. 1. When choosing 8 sites from 54 for substitution, ions will have another ion at least in their second neighbour shell.

For the case of 2 ions in the box, the number of distinct arrangements is smaller. Step 1 was performed for 2000 configurations. Step 3 was performed for thirty configurations.

We have performed steps 3 and 4 using the PWscf program which is part of the Quantum Espresso suite (QE).[33] We use the PBE GGA exchange–correlation functional,[34] a plane wave basis set and ultra-soft pseudo-potentials of type RRKJ3.[35] During geometry optimisation (step 3) internal degrees of freedom, including atomic positions, are moved by a BFGS algorithm until a minimum of the energy is found.[36,37] The energy convergence threshold was 10^{-6} Ry for most boxes, for the few ones which did not converge it was relaxed to 10^{-4} Ry. A few configurations did not converge at all and were discarded. Step 3 was performed on 200 boxes of ice VII with 8 ions and cell parameters of 9.9485 Å. For these values the pressure averages over the set of boxes are 4 GPa. The enthalpies of formation were calculated. The convex hull diagram is given in the ESI.†

During cell optimisation (step 4) the cell parameters are allowed to change in addition to the internal degrees of freedom. The structures were optimised at 4 GPa. We forced the cells to remain cubic, however, small distortions occurred (of the order of 1%). Therefore, another geometry optimisation using the cubic root of the obtained volume as cell parameter was performed subsequently, in order to obtain a cubic structure. Step 4 was performed for 13 boxes of salty ice and for one box of pure ice VII.

An equation of state (EOS) at 0 K was obtained using geometry optimisation where the side of the box ($3a$ where a is the lattice parameter of ice VII) was varied from 9.0 to 11.1 Å for one pure ice box and two boxes with respectively 2 and 8 substituted ions with average behaviour for the sets of step 3. A step of 0.106 Å was chosen between 9.0 and 10.05 Å, above which a value of 0.265 Å was used. The pressure retained is that of the last optimisation cycle. The equations of state $p(a/a_0)$ obtained for a box of pure ice VII, ice VII with one NaCl pair and ice VII with 4 pairs are shown in Fig. 2. The $p(a)$ relation was fitted to a Birch–Murnaghan EOS for the three boxes, in the range of 3.2 to 3.5 Å. The parameters a_0, V_0, B_0, B_0' are given in Table 1

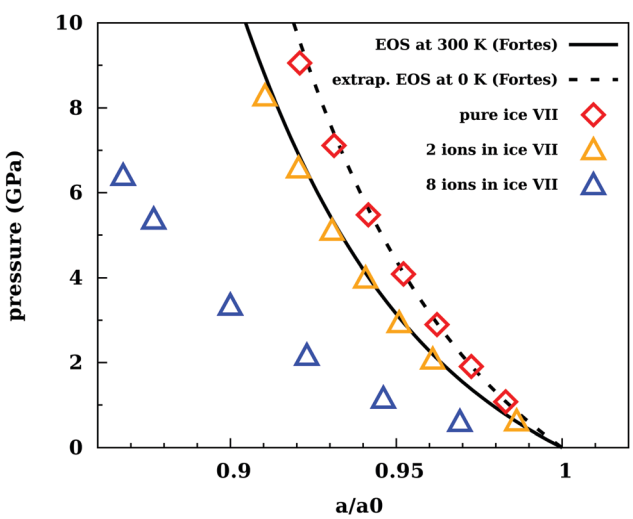

Fig. 2 The equation of state of NaCl-ice VII. The points were obtained from DFT calculations at 0 K. The black line shows the equation of state of pure ice VII from ref. 38 at 300 K, the dashed line shows its extrapolation to 0 K.

Table 1 Parameters of the fits of Birch–Murnaghan equation of state (EOS) to data from simulations, compared to two EOS of ice VII fitted to experiments given in literature.[38,39] M stands for the Murnaghan EOS, BM for the Birch–Murnaghan EOS

System	a_0 (Å)	V_0 (Å^3)	B_0 (GPa)	B_0'
BM ice VII, R = 11.5	3.822	55.83	4.26	6.0
BM ice VII, R = 52	3.4875	42.41	11.98	6.56
BM pure ice VII	3.4095	39.63	18.17	5.68
M pure ice VII (ref. 38)	3.4898	42.5	13.0	5.5
BM ice VII (ref. 39)	3.4580	41.35	20.4	4.7

‡ Where $R = n(H_2O)/n(NaCl)$ is the molar ratio of water molecules to salt pairs.

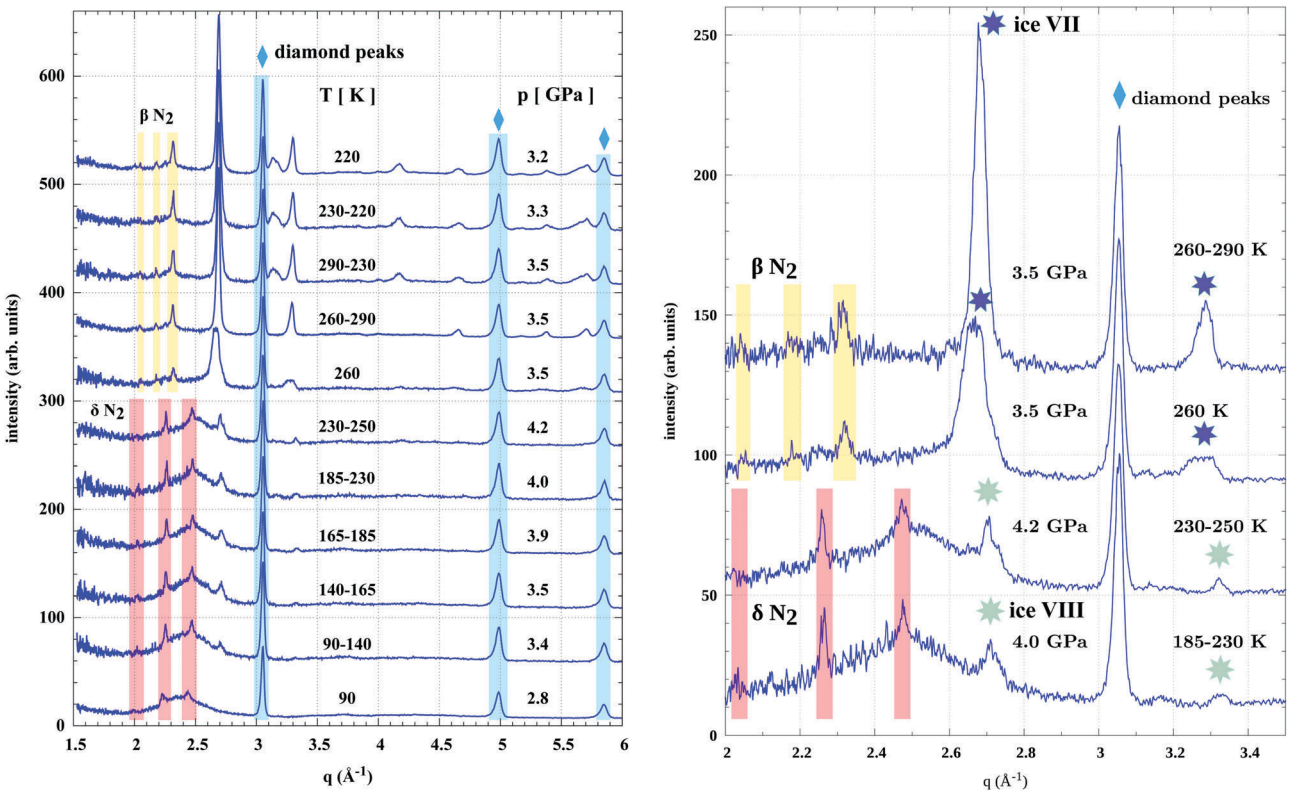

Fig. 3 Crystallisation of ice VII during annealing of sample A at 3.6 GPa. The pressure indicated in both panels corresponds to that of N_2, for details of the pressure measurement see text. Left: Full view of annealing from 90 to 290 K and cooling back to 220 K. The data are in chronological order from bottom to top. Right: Zoom to data from 185 to 290 K. Diamond peaks are indicated by blue diamond symbols, nitrogen phases by vertical bars and ice peaks by green stars for ice VIII and blue stars for ice VII.

and compared to the values from the literature on ice VII. The lines in Fig. 2 correspond to the EOS of ref. 38 for ice VII at 300 K (solid line) and the extrapolation of that EOS to 0 K (dashed line) by accounting for an 18% increase of the bulk modulus with respect to the experimental data at 300 K.

3 Results and discussion

First, we present the crystallisation behaviour of amorphous NaCl·10.2D_2O solution during annealing at high pressure. We discuss the transformations of the sample and the possibility of salt inclusion in the ice lattice. Second, the experimental data are compared to a structural model of ice VII with salt ions substituted for water molecules, which was studied by atomistic simulations.

3.1 Crystallisation upon annealing

The annealing of sample A is shown in Fig. 3. The left hand panel gives an overview of the annealing. Details of the crystallisation of sample A, are shown in the right hand panel, for the scans from 185 to 290 K. At temperatures below 260 K the diffractograms show peaks of the δ phase of N_2 (peaks at 2.2, 2.5 and 2.7 $Å^{-1}$) on top of the amorphous features of NaCl·10.2D_2O. In this sample the pressure, determined from N_2 peaks, varies from 2.8 to 4.2 GPa upon annealing. This is due to the fact that the annealing is isochoric, *i.e.* pressure will increase when temperature increases at constant volume. The peak at 2.7 $Å^{-1}$ appearing at 140 K shows that ice VIII forms from the pure VHDA§ contained in the sample. Before crystallisation, the pressure from the δ phase of N_2 is 4.2 GPa. At 260 K the δ phase transforms into the β phase (new peaks at 2.0, 2.2 and 2.3 $Å^{-1}$) and ice nucleates from the amorphous phase (peaks at 2.65 and 3.25 $Å^{-1}$). Upon crystallisation of ice VII, the pressure, now estimated from the peaks of the β phase, drops to 3.5 GPa. Ice VII has fully crystallised at 290 K. The first ice VII peak at 2.65 $Å^{-1}$ is broader here than what is normally observed in pure ice VII, its FWHM is 0.0297 $Å^{-1}$. Weak salt or hydrate peaks might have appeared at 3.8, 4.0 and 5.17 $Å^{-1}$ at 290 K and 3.65 GPa, but they are hardly identifiable given the level of background noise.

In sample A the crystallisation of the amorphous solution sets in at about 260 K (Fig. 3), close to the phase boundary of ice VIII and VII (270 K). This is very close also to the nucleation temperature of salty ice VII (265 K) from amorphous LiCl·6D_2O at 4 GPa.[7]

The fit of sample A at 290 K and 3.65 GPa is shown in Fig. 4. The fit shown accounts for ice VII, the diamond peaks were fitted and subtracted, and the β N_2 peaks (below 2.4 Å) have also been fitted but this part is not shown by the line in the figure. No peaks of lead are visible. The quality of the fit is good

§ Very-high density amorphous phase of pure water (VHDA), see ref. 40.

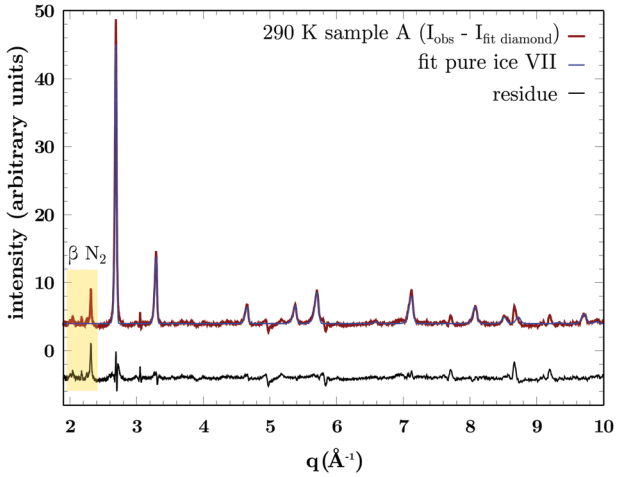

Fig. 4 Rietveld fit of sample A at 290 K and 3.65 GPa with ice VII (χ^2 = 2.775) a = 3.298 Å. No expansion of unit cell found. GSAS was used to perform the fit. The fit of diamond peaks has been subtracted from the experimental data. The peaks of the β phase of N_2 are indicated.

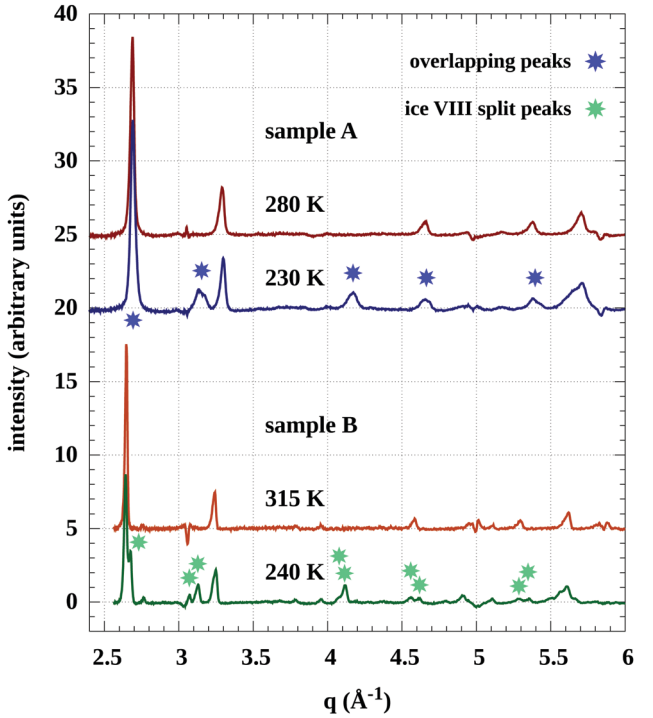

Fig. 5 Formation of ice VIII upon cooling below the phase boundary of ices VII and VIII (270 K) in both samples A (top) and B (bottom). Sample A shows broad overlapping peaks. Sample B shows a clear splitting of the peaks as expected for pure ice VIII. The diamond peaks have been subtracted from the data of both samples.

for a high pressure neutron diffraction experiment, the position of all peaks is reproduced. Texture of the sample was not fitted. The fit of ice VII (χ^2 = 2.775) gives a lattice parameter a = 3.2986 ± 0.0001 Å, which corresponds to a pressure of 3.625 GPa in pure ice.[38] The pressure as determined from the nitrogen phase (3.68 GPa) and ice VII phase agree to better than 0.1 GPa. Although the lattice parameter agrees with that of pure ice VII at this pressure, the ice phase may contain a (small) fraction of salt. If the ions substitute water molecules and occupy oxygen sites, this might explain the lack of expansion of the lattice parameter. Another fit was done using a model of ice VII in which Na^+ and Cl^- ions substitute water molecules with a probability of 1/12.2 each. Since this fit yielded a roughly equal but slightly larger χ^2 value, it is not reported here. The data and fit are shown in Fig. S1 and S2 of the ESI.†

Next, the sample was cooled down from 290 to 230 K to see whether it would transform to ice VIII, as shown in the upper half of Fig. 5. Ice VIII is a hydrogen ordered phase, hence we expect that the transition does not occur if the salt is included in the ice structure, as is the case in ice VII that contains LiCl salt.[7] In sample A the splitting of the 110 and 211 peaks is not clear-cut, however the broad feature at $q \approx 3.2$ Å^{-1} with FWHM = 0.0372 Å^{-1} corresponds to two ice VIII peaks (103 and 211). Another peak appears at $q \approx 4.2$ Å^{-1} (213 and 301). These broad features may be an indication that this could be a disordered form of ice VIII, which might have incorporated ions. It might also be due to the superposition of peaks of ice VIII and peaks of salty ice VII. We try to quantify the amount of ions included with the help of our simulations (see Section 3.2).

The annealing of sample B is shown in Fig. 6. At temperatures below 165 K the diffractograms show peaks of the δ phase of N_2 on top of the amorphous features of NaCl·10.2D_2O. At 165 K the δ phase transforms into the β phase and ice VIII forms from the pure VHDA in the sample. From the β phase a pressure of 2.5 GPa can be estimated. At 220 K a strong peak appears at 2.65 Å^{-1} and a smaller one at 3.25 Å^{-1}. These peaks grow from 240 to 255 K. This phase is ice VIII, which can be seen from the shoulder at ≈2.7 Å^{-1} and the peak at 3.15 Å^{-1}. At 270 K both the shoulder and the next peak disappear, indicating that the sample has transformed into ice VII. This peak is narrower here than in samples A and C, its FWHM is 0.0186 Å^{-1}, which is a clear indication that this sample is pure ice VII. This is confirmed by the presence of salt peaks which can be seen at 1.98, 2.29, 3.80, 3.96 and 5.11 Å^{-1}. Fitting the salt peaks (and lead) gives a pressure of 2.25 ± 0.03 GPa. The same pressure is obtained by using the EOS of ref. 38 and the lattice parameter obtained from the fit of ice VII (3.35 Å).

At 240 K the peaks of the β phase start to weaken, probably due to melting. This indicates a slight loss of pressure, in agreement with the pressure obtained from the salt peaks. In sample B, pressure loss occurs in two steps, first a drop of 0.3 GPa as ice VIII crystallises at about 170 K. The second step is a pressure loss of about 0.4 GPa from 220 to 270 K.

Starting at 240 K, several peaks appear in the region from 2 to 2.5 Å^{-1}. They grow upon annealing to 300 K. Two of these are the salt peaks mentioned above. The phase, to which the other peaks at 2.20, 2.23, 2.47 and a weaker one at 2.76 Å^{-1} belong, has not been identified. They may belong to a mixed phase of salt or nitrogen hydrate.

The fit of sample B at 300 K and 2.25 GPa is shown in Fig. 7. Salt peaks are visible here. A fit for lead peaks has been attempted, but they are weak. A fit including ice VII, diamond, sodium chloride and lead has been performed, only the ice VII

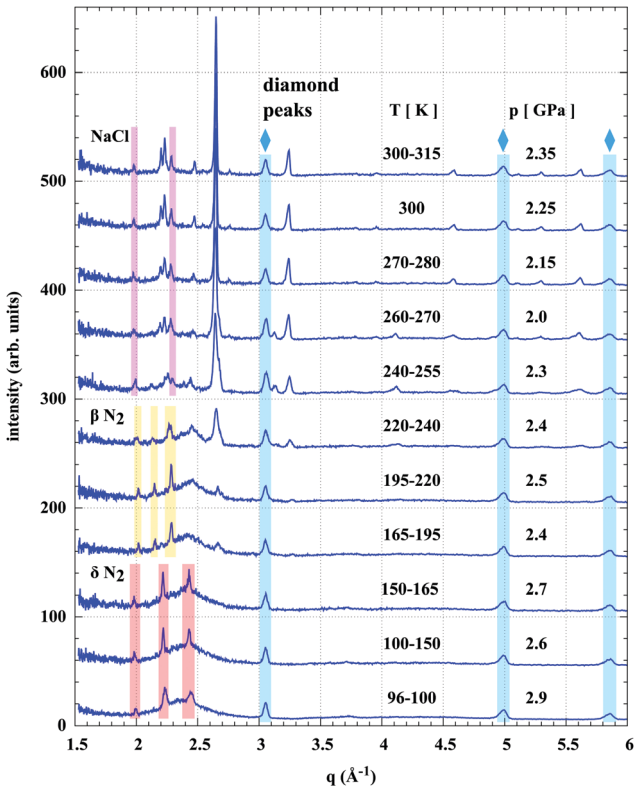

Fig. 6 Annealing of sample B from 96 to 315 K. Ice VIII crystallises at 220 K and 2.4 GPa. At 270 K ice VIII transforms into ice VII. For the details of pressure measurement see text.

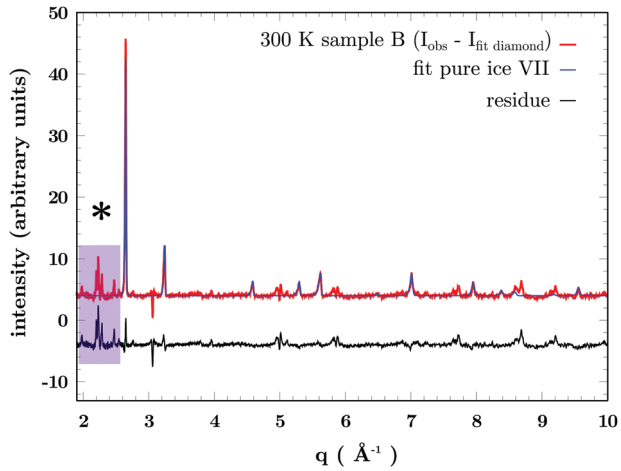

Fig. 7 Rietveld fit of sample B in which pure ice VII crystallises at 300 K and 2.25 GPa. The fit of diamond peaks has been subtracted from the experimental data. The peaks beneath the asterisk do not belong to ice, refer to the discussion in the text.

contribution is shown in the figure. The fit of ice VII with GSAS (χ^2 = 1.910) gives a lattice parameter a = 3.3507 ± 0.0001 Å, which corresponds to a pressure of 2.25 GPa in pure ice.[38] The pressure of the lead (2.23 GPa), NaCl (2.28 GPa) and ice VII phase agree to less than 0.1 GPa. Hence this sample contains pure ice VII.

Sample B clearly shows the transition to ice VIII. Upon cooling the splitting characteristic of ice VIII appears on the 110 and 211 peaks as shown in Fig. 5. Also, the pairs at $q \approx 2$ Å^{-1} (103 and 211) and $q \approx 1.5$ Å^{-1} (213 and 301) appear clearly split.

Sample C behaves like sample A. A small amount of ice VIII forms at 120 K and grows slightly until 260 K. The amorphous phase remains present in the sample up to 260 K. Ice VII crystallized at 260 K during annealing at ≈4 GPa. The fit of ice VII (χ^2 = 1.130) gives a lattice parameter a = 3.28912 ± 0.00014 Å for the cubic unit cell of the oxygen lattice. This is compared to the results for sample A and B in Table 2.

The results for the fits of ice VII in samples A, B and C are summed up in Table 2. The Debye–Waller factors quantify the average displacement of atoms from the crystallographic sites. This can be due to either thermal motion or static disorder. The values of the isotropic Debye–Waller factor U_{iso} obtained from the fits of samples A, B and C are given in Table 2. For sample A and C they are in good agreement with those of pure ice.[41] The values obtained for sample B are larger than those of ref. 41. This is probably due to the fact that the pressure is less than half of that in their experiment.[41]

The width of the peaks can be due to several factors. Particle size, strain and inclusion of salt ions are possible explanations. The most probable cause is particle size here, given the lack of expansion of the unit cell. The crystallites forming at higher pressure are usually smaller than those forming at lower pressure. The particle size s was obtained from the fits using the Scherrer formula as given by ref. 21

$$s = \frac{CK}{\sqrt{8\ln(2)\sigma_2^2}} \quad (1)$$

where C = 4834.55 μs is the diffractometer constant, $K \approx 0.9$ is the Scherrer constant and σ_2 is a profile parameter. The particle sizes for ice VII fits of samples A, B and C are given in Table 2. This estimation of the particle size gives the average size of the grains of ice crystals in the sample. In sample A the fit gives the smallest particle size of only 360 Å (36 nanometres). In sample B it is largest at about 610 Å.

To summarise, the data show that sample B forms pure ice VII. For samples A and C the data and fits alone are not sufficient to establish, whether part of the crystalline sample has included salt into the ice VII lattice, since salt peaks are barely visible in all scans and the transition to ice VIII upon lowering the temperature is not clearly observed. To complement our study we present a model of salty ice VII in which ions are substituted for water molecules.

3.2 Structure and stability of salty ice VII

In the model of salty ice proposed here the ions are all included by substituting water molecules. The substitutional structure is shown below the pure ice VII structure in the inset of Fig. 1. In the following we present the equation of state obtained for this structure and the structure factors calculated from simulations.

As can be seen from Table 1 the volume at zero pressure V_0 increases with salt content (decreasing R). Moreover, the salty ices have a smaller bulk modulus B_0 and therefore they are more compressible. The B_0 of the ice with 8 ions is even smaller

Table 2 Results of the Rietveld fits with GSAS[20] for samples A, B and C. The lattice parameters, the pressures (by EOS of ref. 38), the profile parameter σ_2 and the ice particle size s for ice VII are given. These pressures agree well with those obtained by fitting the pressure probes (Pb, N_2, NaCl). The estimated standard error of the lattice parameter is given in parenthesis after the last digit. The uncertainty of the pressure estimate is $\approx \pm 0.1$ GPa. Isotropic Debye–Waller factors of oxygen (O) and deuterium (D) for the ice phases crystallised from the samples are given. The Debye–Waller factors obtained by ref. 41 on pure deuterated ice VII are given for comparison

		Ice VII						*p*-Marker	
Sample	T (K)	a (Å)	p (GPa)	σ_2^2 (μs^2 Å^{-2})	s (Å)	U_{iso}(O) (Å^2)	U_{iso}(D) (Å^2)	p (GPa)	Phase
A	290	3.2986(1)	3.62 ± 0.1	27.0	360	0.017	0.022	3.68 ± 0.1	(β N_2)
B	300	3.3507(1)	2.26 ± 0.1	9.0	610	0.022	0.030	2.25 ± 0.1	(NaCl + Pb)
C	300	3.2892(1)	3.91 ± 0.1	17.0	450	0.015	0.026	3.94 ± 0.1	(Pb)

		Ice VII			
Sample	T (K)	p (GPa)	U_{iso} (O) (Å^2)	$U_{\perp}$ (D) (Å^2)	$U_{\parallel}$ (D) (Å^2)
Ref. 41	290	5	0.018	0.027	0.017

than that of the δ phase of N_2 (5.75 GPa after ref. 25). The comparatively smaller bulk modulus is also seen in the deviation of the data obtained from the simulation with 8 ions (blue triangles), from the data for pure ice VII in Fig. 2.

From the *ab initio* calculations on the ice VII with NaCl, we find an expansion of the unit cell, when comparing boxes where ions are included to the box of pure ice VII. For salty ice with R = 52 (2 ions) at 4 GPa the expansion is $\Delta a/a$ = 1.1% in the box size and $\Delta v/v$ = 3.2% in volume for the single box used for the EOS. For the box of salty ice with R = 11.5 (8 ions) at 4 GPa the expansion is $\Delta a/a$ = 4.2% in the box size of our simulation and $\Delta v/v$ = 13% in volume for the box which was used for the EOS. For the set of 200 hydrogen disordered boxes for which geometry optimisation was performed, the optimisation of a box chosen close to the average pressure of the set gives an expansion of $\Delta a/a$ = 3.2% in the box size and $\Delta v/v$ = 10% in volume. Given these values for the expansion of salty ice VII, it would be expected that the samples measured would only include a small fraction of ions in their lattice, since they show much smaller expansion compared to pure ice VII. It should be noted that the boxes sampled in our *ab initio* calculations are small, and that, moreover, the equation of state was obtained for single boxes only. The spread in pressure at fixed box size for the boxes generated by random searching is of ±0.4 GPa. Thus the two boxes chosen may not be representative for the behaviour of all boxes, but they were chosen to be representative of the average behavior of the set. Nevertheless, the fact that the boxes expand more when they contain more ions, is consistent with what would be expected by analogy with the case of LiCl solution, where salt inclusion (substitutional for Cl^- and interstitial for Li^+) also leads to expansion.

Fig. 8 shows the experimental diffraction pattern of sample A at 290 K and 3.65 GPa (blue line at the top) in comparison to different models of ice VII. The fit of the background and diamond peaks, obtained by fitting the pattern with GSAS, was subtracted from experimental data (blue). The β nitrogen (peak at 2.4 Å^{-1}), which was also fitted, has not been removed in this diffractogram. The FullProf model (dark blue) is the same bcc structure as was used in the GSAS fit (a = 3.2986 Å). The relative intensities differ from those in the experimental diffractogram, because this model is not a fit. Here the program

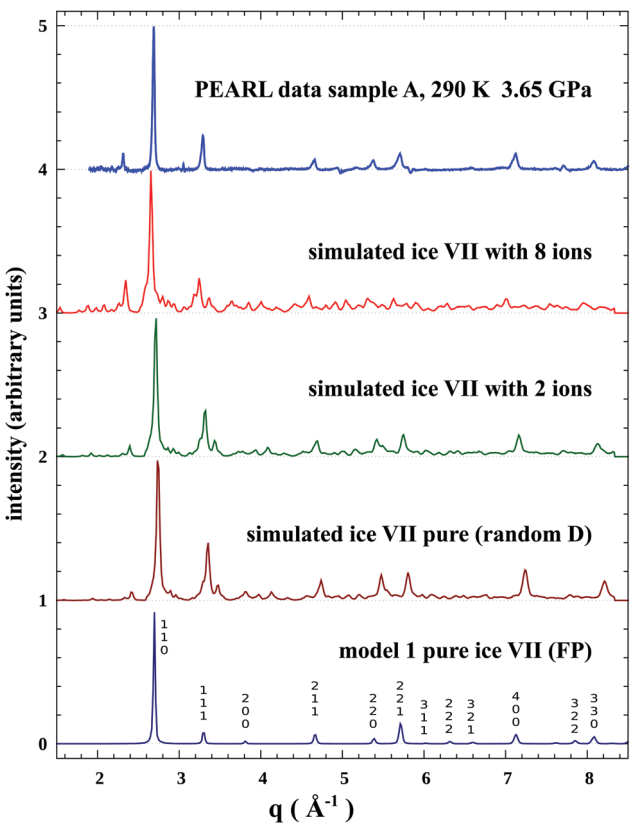

Fig. 8 Diffraction pattern of crystallised sample A compared to structure factors (SF) calculated with a FullProf model of pure ice (dark blue at bottom) and three models from simulations (red and dark-green). In all models, all water is assumed to be D_2O. The dark red SF corresponds to a pure ice VII box with disorder of deuterium, the dark green to a box containing 2 ions (R = 52), the red to a box with 8 ions (R = 11.5). The dark red and dark green SF show better agreement with the experimental data. The Miller indices are shown on the FullProf model at the bottom.

assumes that all possible sites for deuterium have an occupation of 1/2. The Miller indices of twelve visible ice VII peaks are indicated on the figure.

The other three diffractograms were produced by FullProf using the boxes from our simulations as unit cells with space

group $P1$, all isotropic displacement factors were taken as $B = 1$ Å^2. The diffractogram labelled pure ice (dark red) was produced using the supercell containing only water molecules, in which the deuterium atoms are disordered. This diffractogram shows all peaks of ice VII which appear in the Fullprof fit with reasonable intensities. The 110 peak shows a shoulder at the right side (towards larger q). This diffractogram also shows small spurious peaks at $\approx$2.4, 3.4, 4.0 and 4.1 Å^{-1} due to periodic boundary conditions. The pattern of the box containing 2 ions (dark green) is very similar that of pure ice VII. Both patterns show seven recognisable peaks for $2 \leq q \leq 8.5$ Å^{-1}, they are 110, 111, 200, 211, 221, 400, 330. The box sizes at 4 GPa were used to produce these diffractograms, this is why the peaks are slightly shifted with respect to the FullProf model and the experimental data. In the pattern for the box containing 8 ions (red), the 110 peak is broader than in other models and the diffractogram of sample A, and only one other peak 111 is well defined. This 111 peak is only half as strong as that in the pure ice model. The other 5 peaks are weak and start to merge into the background. This pattern shows less resemblance to the experimental diffractogram than the other models. However, these features described above are similar to those of salty ice VII crystallized from $LiCl{\cdot}6D_2O$.[7]

From these structure factors the most plausible models for the measured diffractogram are pure ice (model in dark red and dark blue) and ice with few ions (model in dark green). This means that the molar ratio R is considerably larger than 11.5 (model in red), possibly even as large as 52 (model in dark green). Hence, most of the salt would have been excluded from the ice lattice.

The stability of these ices was probed by calculating the enthalpy of mixing Δh per site of the oxygen lattice using the DFT calculations. The convex hull diagram of enthalpies (see Fig. S3, ESI†) shows that the configurations for which geometry optimisation was performed have enthalpies larger than those of the separated ice and salt. This indicates that the salty ice is unstable, but it may be metastable on the experimental time scale.

The quantity Δh was computed from DFT geometry optimisation on 200 boxes of lowest DFT energy. The configurations were filtered to lie within 0.1 GPa of 4 GPa. The average of Δh is about 0.0055 Ry and its spread of the order of 0.002 Ry, which corresponds to $\approx$315 K. This suggests that the thermal energy at 300 K would be sufficient to allow the system to relax to the stable state of pure ice VII and salt.

4 Conclusions and perspectives

The analysis of our diffraction data suggests that the ice VII which crystallised upon annealing at 2.5 and 4 GPa contains little or no salt in its lattice. This is supported by the lattice parameters and Debye–Waller factors, which are in good agreement with the literature data on pure ice VII. However, crystallization takes place at much higher temperatures and/or pressures than expected and directly into the proton disordered ice VII phase. In other words, the amorphous phase extends over a broad p–T domain where pure water crystallizes into ordered phase VIII. The broadening of peaks observed in two samples could be due to the small size of crystallites formed by the crystallization from the amorphous precursor. Our calculations show that substituting ions into the lattice of ice VII should lead to an expansion of the unit cell by about 10% in volume, if all of the salt in the sample were included in the ice at 0 K. The computed structure factors of salty ice show strong Debye–Waller factors at high salt concentration, which is at variance with our experimental observations. Analysis of the enthalpies of mixing obtained from the set of candidate structures shows that salty ice would be at the verge of stability at 300 K and 4 GPa.

Therefore, the crystalline ice formed in ice layers which remain below 4 GPa, for instance in moons, would include only small amounts of rock salt in its structure, our neutron diffraction experiments give an upper bound for the amount of salt that may be included. Thus the known equation of state of pure ice VII may be used as a reasonable approximation to model the internal structure of such icy bodies.

The behaviour of the system at higher pressures (*i.e.* above 5 GPa) but below the transition to ice X may be different from the behaviour observed in this work. As NaCl-ice samples obtained by annealing of a dilute amorphous precursor ($NaCl{\cdot}52H_2O$) at much higher pressures (about 10 GPa) show effects compatible with a likely inclusion of salt in the ice lattice,[9] it is possible that higher pressures than the ones investigated in this study or lower salt concentrations are needed to keep the NaCl in the ice structure. This hypothesis is the object of a forthcoming study. It would also be worthwhile to investigate these higher pressures, because they occur in the interiors of massive planetary bodies such as super-earths and ice giants.[42]

Acknowledgements

We thank Ludovic Delbes at IMPMC for technical assistance. We are grateful to Robert Pick and Richard Gaal for fruitful discussions and assistance. This work was supported by French state funds managed by the ANR within the Blanc International programme PACS under reference ANR-13-IS04-0006-01 and the Investissements d'Avenir programme under reference ANR-11-IDEX-0004-02, within the framework of the Cluster of Excellence MATériaux Interfaces Surfaces Environnement (MATISSE) led by Sorbonne Universités, and by the Swiss National Science Foundation through the FNS Grant 200021-149847. A. L. thanks Betül Pamuk, Zamaan Raza and Ivo Rietveld for fruitful advice. We thank the STFC for access to the ISIS facility and technical support. This work is based on experiments performed at the ISIS spallation source, Didcot, UK, as well as on calculations performed on the GNOME cluster at UPMC and on the Occigen cluster at CINES, Montpellier, France, under DARI references 2014-091387 and 2015-091387.

References

1 A.-A. Ludl, L. E. Bove, A. M. Saitta, M. Salanne, T. Hansen, C. L. Bull, R. Gaal and S. Klotz, *Phys. Chem. Chem. Phys.*, 2015, 14054–14063.

2 W. F. Kuhs, C. Sippel, A. Falenty and T. C. Hansen, *Proc. Natl. Acad. Sci. U. S. A.*, 2012, **109**, 21259–21264.

3 L. Bove, S. Klotz, J. Philippe and A. Saitta, *Phys. Rev. Lett.*, 2011, **106**, 125701.
4 L. X. Dang and T.-M. Chang, *J. Chem. Phys.*, 1997, **106**, 8149–8159.
5 S. Tazi, J. J. Molina, B. Rotenberg, P. Turq, R. Vuilleumier and M. Salanne, *J. Chem. Phys.*, 2012, **136**, 114507.
6 S. Klotz, K. Komatsu, F. Pietrucci, H. Kagi, A.-A. Ludl, S. Machida, T. Hattori, A. Sano-Furukawa and L. E. Bove, *Sci. Rep.*, 2016, **6**, 32040.
7 S. Klotz, L. E. Bove, T. Strässle, T. C. Hansen and A. M. Saitta, *Nat. Mater.*, 2009, **8**, 405–409.
8 B. Pamuk, P. B. Allen and M.-V. Fernández-Serra, *Phys. Rev. B: Condens. Matter Mater. Phys.*, 2015, **92**, 134105.
9 Y. Bronstein, P. Depondt, L. E. Bove, R. Gaal, A. M. Saitta and F. Finocchi, *Phys. Rev. B*, 2016, **93**, 024104.
10 K. Komatsu, A. Shinozaki, S. Machida, T. Matsubayashi, M. Watanabe, H. Kagi, A. Sano-Furukawa and T. Hattori, *Acta Crystallogr., Sect. B: Struct. Sci., Cryst. Eng. Mater.*, 2015, **71**, 74–80.
11 L. E. Bove, R. Gaal, Z. Raza, A.-A. Ludl, S. Klotz, A. M. Saitta, A. F. Goncharov and P. Gillet, *Proc. Natl. Acad. Sci. U. S. A.*, 2015, **112**, 8216–8220.
12 M. R. Frank, C. E. Runge, H. P. Scott, S. J. Maglio, J. Olson, V. B. Prakapenka and G. Shen, *Phys. Earth Planet. Inter.*, 2006, **155**, 152–162.
13 L. Bezacier, B. Journaux, J.-P. Perrillat, H. Cardon, M. Hanfland and I. Daniel, *J. Chem. Phys.*, 2014, **141**, 104505.
14 C. A. Angell and E. J. Sare, *J. Chem. Phys.*, 1970, **52**, 1058.
15 A.-A. Ludl, L. E. Bove, J. Li, M. Morand and S. Klotz, *Eur. Phys. J.: Spec. Top.*, accepted.
16 C. L. Bull, N. P. Funnell, M. G. Tucker, S. Hull, D. J. Francis and W. G. Marshall, *High Pressure Res.*, 2016, **36**, 493–511.
17 T. Strässle, S. Klotz, K. Kunc, V. Pomjakushin and J. S. White, *Phys. Rev. B: Condens. Matter Mater. Phys.*, 2014, **90**, 014101.
18 W. G. Marshall and D. J. Francis, *J. Appl. Crystallogr.*, 2002, **35**, 122–125.
19 S. Klotz, *Techniques in High Pressure Neutron Scattering*, Taylor & Francis, Boca Raton, Florida, 2013, ch. 11, pp. 141–145.
20 A. C. Larson and R. B. Von Dreele, *General Structure Analysis System*, LANSCE, MS-H805, Los Alamos, New Mexico, 1994.
21 A. Larson and R. Von Dreele, *Report LAUR*, 2000.
22 B. H. Toby, *J. Appl. Crystallogr.*, 2001, **34**, 210–213.
23 W. F. Kuhs, J. L. Finney, C. Vettier and D. V. Bliss, *J. Chem. Phys.*, 1984, **81**, 3612.
24 J. D. Jorgensen and T. G. Worlton, *J. Chem. Phys.*, 1985, **83**, 329.
25 R. Mills, B. Olinger and D. Cromer, *J. Chem. Phys.*, 1986, **84**, 2837–2845.
26 W. E. Streib, T. H. Jordan and W. N. Lipscomb, *J. Chem. Phys.*, 1962, **37**, 2962.
27 G. W. Stinton, I. Loa, L. F. Lundegaard and M. I. McMahon, *J. Chem. Phys.*, 2009, **131**, 104511.
28 S. Klotz, G. Hamel, J. Loveday, R. Nelmes and M. Guthrie, *Z. Kristallogr.*, 2003, **218**, 117–122.
29 D. Corradini, D. Dambournet and M. Salanne, *Sci. Rep.*, 2015, **5**, 11553.
30 C. E. Wilmer, M. Leaf, C. Y. Lee, O. K. Farha, B. G. Hauser, J. T. Hupp and R. Q. Snurr, *Nat. Chem.*, 2011, **4**, 83–89.
31 F.-X. Coudert, *Phys. Chem. Chem. Phys.*, 2013, **15**, 16012.
32 C. Developers Group, CP2K website, CP2K Developers Group, 2012.
33 P. Giannozzi, S. Baroni, N. Bonini, M. Calandra, R. Car, C. Cavazzoni, D. Ceresoli, G. L. Chiarotti, M. Cococcioni, I. Dabo, A. D. Corso, S. de Gironcoli, S. Fabris, G. Fratesi, R. Gebauer, U. Gerstmann, C. Gougoussis, A. Kokalj, M. Lazzeri, L. Martin-Samos, N. Marzari, F. Mauri, R. Mazzarello, S. Paolini, A. Pasquarello, L. Paulatto, C. Sbraccia, S. Scandolo, G. Sclauzero, A. P. Seitsonen, A. Smogunov, P. Umari and R. M. Wentzcovitch, *J. Phys.: Condens. Matter*, 2009, **21**, 395502.
34 J. P. Perdew, K. Burke and M. Ernzerhof, *Phys. Rev. Lett.*, 1996, **77**, 3865–3868.
35 A. M. Rappe, K. M. Rabe, E. Kaxiras and J. D. Joannopoulos, *Phys. Rev. B: Condens. Matter Mater. Phys.*, 1990, **41**, 1227–1230.
36 R. Fletcher, *Optimization*, 1987, **1**, 784–794.
37 S. R. Billeter, A. Curioni and W. Andreoni, *Comput. Mater. Sci.*, 2003, **27**, 437–445.
38 A. D. Fortes, I. G. Wood, M. G. Tucker and W. G. Marshall, *J. Appl. Crystallogr.*, 2012, **45**, 523–534.
39 J. Besson, P. Pruzan, S. Klotz, G. Hamel, B. Silvi, R. Nelmes, J. Loveday, R. Wilson and S. Hull, *Phys. Rev. B: Condens. Matter Mater. Phys.*, 1994, **49**, 12540.
40 R. J. Nelmes, J. S. Loveday, T. Strässle, C. L. Bull, M. Guthrie, G. Hamel and S. Klotz, *Nat. Phys.*, 2006, **2**, 414–418.
41 R. J. Nelmes, J. S. Loveday, W. G. Marshall, G. Hamel, J. M. Besson and S. Klotz, *Phys. Rev. Lett.*, 1998, **81**, 2719–2722.
42 J.-P. Beaulieu, D. P. Bennett, P. Fouqué, A. Williams, M. Dominik, U. G. Jørgensen, D. Kubas, A. Cassan, C. Coutures, J. Greenhill, K. Hill, J. Menzies, P. D. Sackett, M. Albrow, S. Brillant, J. A. R. Caldwell, J. J. Calitz, K. H. Cook, E. Corrales, M. Desort, S. Dieters, D. Dominis, J. Donatowicz, M. Hoffman, S. Kane, J.-B. Marquette, R. Martin, P. Meintjes, K. Pollard, K. Sahu, C. Vinter, J. Wambsganss, K. Woller, K. Horne, I. Steele, D. M. Bramich, M. Burgdorf, C. Snodgrass, M. Bode, A. Udalski, M. K. Szymański, M. Kubiak, T. Wieckowski, G. Pietrzyński, I. Soszyński, O. Szewczyk, Ł. Wyrzykowski, B. Paczyński, F. Abe, I. A. Bond, T. R. Britton, A. C. Gilmore, J. B. Hearnshaw, Y. Itow, K. Kamiya, P. M. Kilmartin, A. V. Korpela, K. Masuda, Y. Matsubara, M. Motomura, Y. Muraki, S. Nakamura, C. Okada, K. Ohnishi, N. J. Rattenbury, T. Sako, S. Sato, M. Sasaki, T. Sekiguchi, D. J. Sullivan, P. J. Tristram, P. C. M. Yock and T. Yoshioka, *Nature*, 2006, **439**, 437–440.